SUPPLEMENTARY METHODS

Non-contrast computed tomography (NCCT) imaging acquisition

A 64-slice dual-source CT scanner (Siemens, Somatom Definition, Germany) was used for the NCCT scan. The scanning range was from the skull base to the top with scan thickness of 5 mm, a tube current of 550~600 mAs, a tube voltage of 120 KV, a field of view (FOV) of 25 cm, and a matrix size of 512 × 512.

Handcrafted radiomics feature

Handcrafted radiomics features were computed from the radiologist-drawn regions of interest (ROIs) using an open-source python package PyRadiomics (version 2.1.2) on hepatoma and perihematomal edema (PHE) volumes, respectively. The online documentation of PyRadiomics package depicts the detailed formation of radiomics features (https://pyradiomics.readthedocs.io/en/latest/features.html). We set resampled voxel sizes as 1× 1 × 1 mm^3 voxels for the slice thickness standardization, the bin width of image intensities as 25 HU, and voxel array shift as 1000. To allow the involvement of the whole tumor and avoid interference from the air and bone tissues, segmented voxels were resampled with the range of 50 to 400 HU. Defined radiomic image features without/with wavelet filtration were extracted to interpret tumor characteristics comprehensively. Wavelet filtration filtered original image with two pass filters, high pass filter (H) and low pass filter (L) for three directions, x, y and z respectively, which represented a total of eight different combinations of decompositions. The extracted radiomics features could be classified into three groups: (a) first-order statistics, (b) shape features, (c) second-order statistics. Most radiomics features mentioned above showed consistency with feature definitions in accordance with the IBSI guidelines (available document online).

There are differences in gray value discretization for the fixed bin size type and resampling, both of which cannot be corrected by customization settings alone and require replacement by custom functions (shown in the Pyradiomics documents). There are two features available in PyRadiomics without definitions in the IBSI, Total Energy and Standard Deviation. Entropy in Pyradiomics is defined by IBSI named Intensity Histogram Entropy. Uniformity in Pyradiomics is defined by IBSI named Intensity Histogram Uniformity. Mesh Volume in Pyradiomics is defined named Volume. Voxel Volume in Pyradiomics is defined in IBSI named Approximate Volume. Joint Energy in Pyradiomics is defined by IBSI named Angular Second Moment. Maximum Probability in Pyradiomics is defined by IBSI named Joint maximum. Sum of Squares in Pyradiomics is defined by IBSI named Joint Variance. The PyRadiomics kurtosis is not corrected, whereas IBSI kurtosis is corrected by -3, yielding 0 for normal distributions. Despite these features above, the remaining features are consistent with the IBSI definitions.

Deep learning features

Imaging preprocessing: With the masked delineation of ROIs for hematoma and PHE, we adjust the size of three consecutive axial slices with maximum tumor into 224 mm * 224 mm for the input layer of the convolutional neural networks (CNNs) models using a bounding box covering the whole tumor area. The resized images with 3 consecutive axial slices as image channels would be candidate of the CNNs for feature extraction.

CNNs architecture: A total of six base models were applied on hematoma and PHE respectively for the extraction of deep learning features with representativeness, including Xception, VGG16, VGG19, ResNet50, InceptionV3, and InceptionResNetV2. These six CNNs were commonly used and pre-trained by the large-scale and well-annotated ImageNet database. This published research

released dataset containing enormous object categories and manually annotated training images, the optimization hyperparameters of which was not tuned permitting a broader generalization on other datasets. After preprocessing, prepared slices of NCCT images with the maximum axial area of the tumor lesion would be ready as the input of the pre-trained CNNs to generate deep learning features. The models are publicly accessed by Keras and TensorFlow open-source code (https://github.com/fchollet/deep-learning-models/).

Elimination of the last fully-connected layer:

The convolutional base is connected by a fully-connected layer for the pre-trained models. We removed the last fully-connected layer, and then different CNNs reached various numbers of feature maps (2048 for ResNet50, InceptionV3 and Xception, 512 for VGG16 and VGG19, and 1536 for InceptionResNetV2) from the new output of these models.

Addition of max pooling layer and feature extraction: With the utility of a global pooling window, local data would be concentrated into a decreased dimensionality. After Step 3.3, for models with more than one-dimensional features, we got feature maps with height and width dimensions corresponding to location invariance in the input layer. After global max pooling, each feature map vector was transformed to a maximal raw value among them. During this step, the feature maps were transformed to numeric values, as representational deep learning features.

Statistical analysis

Feature robustness for inter-observer reproducibility was assessed by intra-class correlation coefficients (ICCs) using "irr" R package. Discrimination abilities were tested by Harrell's concordance indices (C-index) and calibration curves using "rms" and "Hmisc" R packages. The depiction of nomogram was depicted by "Hmisc" package. The decision curve analysis was performed by "rmda" R package.

Handcrafted radiomic model (Hemorrhage- or edema-derived features)

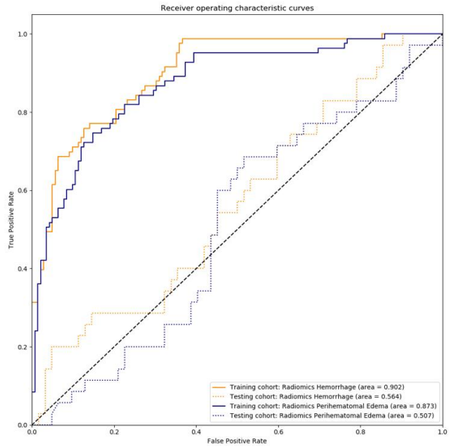

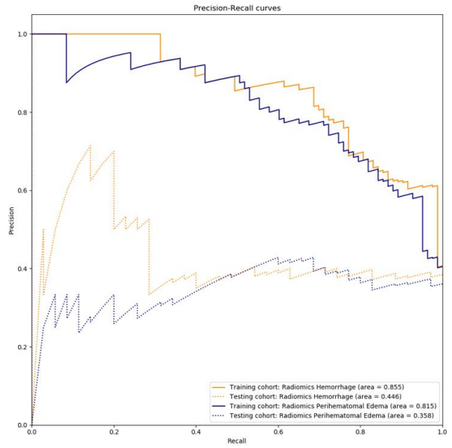

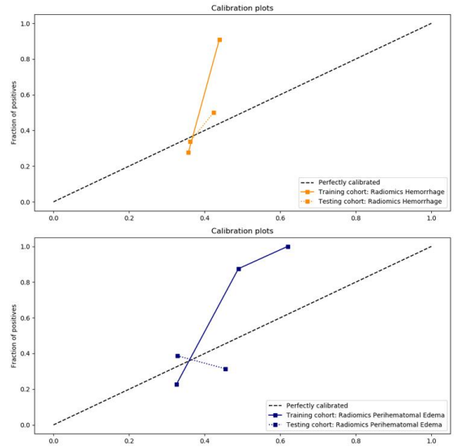

Handcrafted radiomic model (Combining hemorrhage- and edema-derived features)

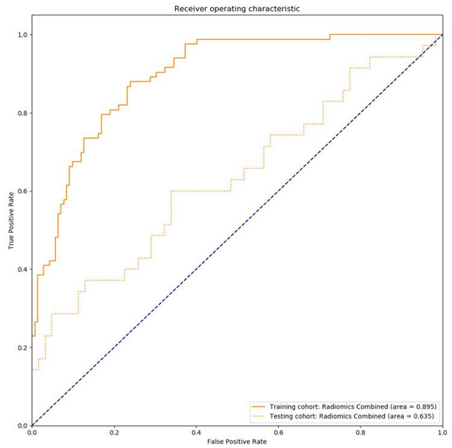

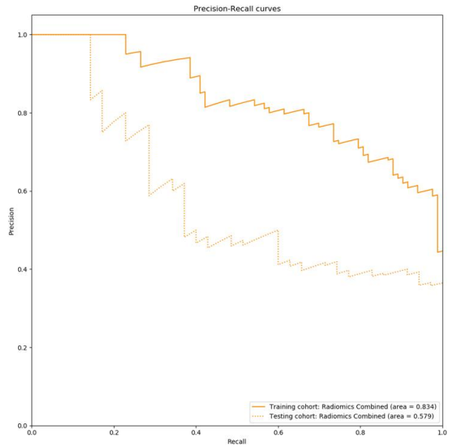

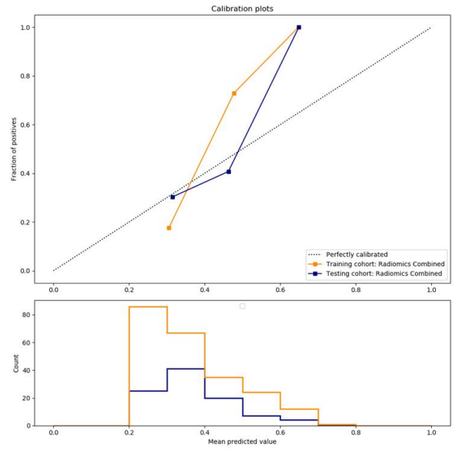

ROC curve **Precision-recall plot** **Calibration plot**

Supplementary Figure 1 Evaluation of predictive performance of handcrafted radiomics models in prediction of early enlargement of spontaneous intracerebral hemorrhage on patients in the training and testing cohorts. Evaluation of predictive performances for handcrafted radiomics models using hemorrhage-derived, perihematomal edema-derived, and combined features by ROC analysis, precision-recall plots, and calibration analysis. ROC, Receiver operating characteristic.

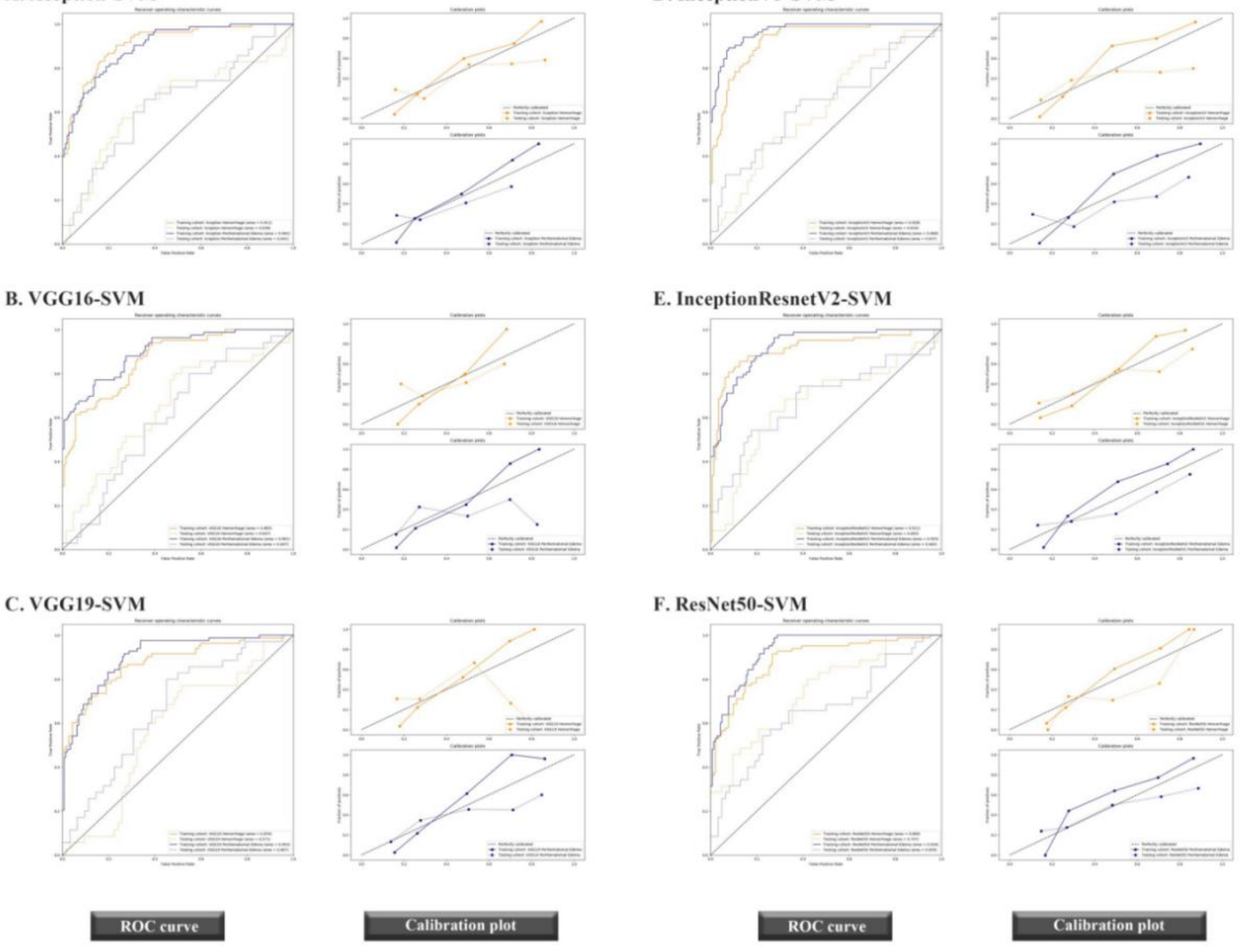

Supplementary Figure 2 Evaluation of predictive performance of DL-SVM models on hemorrhage- or perihematomal edema-derived features in prediction of early enlargement of spontaneous intracerebral hemorrhage on patients in the training and testing cohorts. Evaluation of predictive performances for DL-SVM models using hemorrhage-derived or perihematomal edema-derived DL-associated features by ROC analysis and calibration analysis. DL, Deep learning; SVM, Support vector machine; ROC, Receiver operating characteristic.

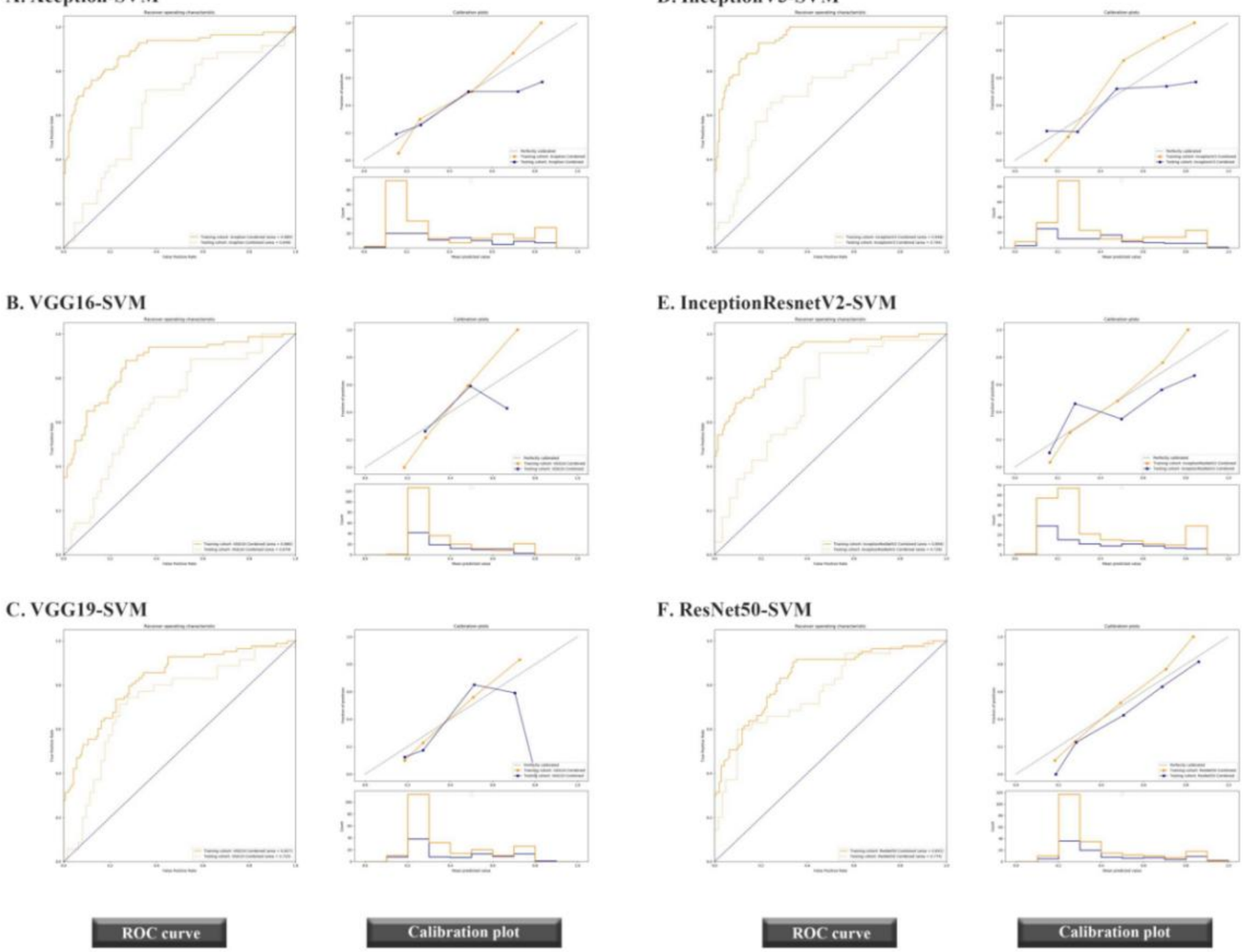

Supplementary Figure 3 Evaluation of predictive performance of DL-SVM models combining hemorrhage- and perihematomal edema-derived features in prediction of early enlargement of spontaneous intracerebral hemorrhage on patients in the training and testing cohorts. Evaluation of predictive performances for DL-SVM models integrating hemorrhage- and perihematomal edema-derived features DL-associated features by ROC analysis and calibration analysis. DL, Deep learning; SVM, Support vector machine; ROC, Receiver operating characteristic.

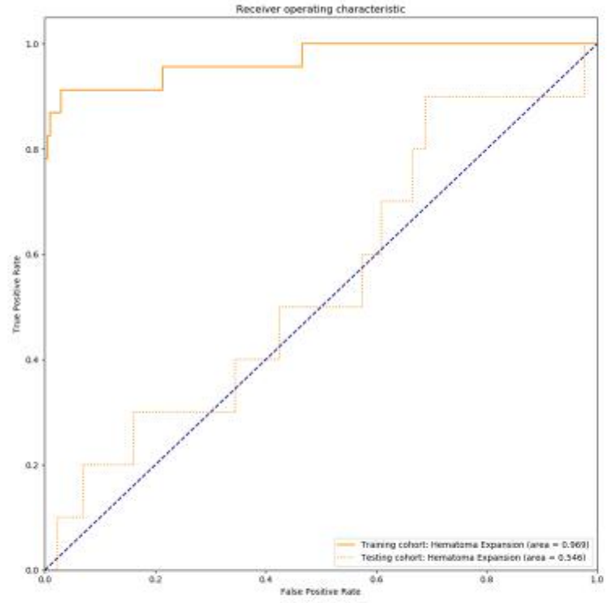

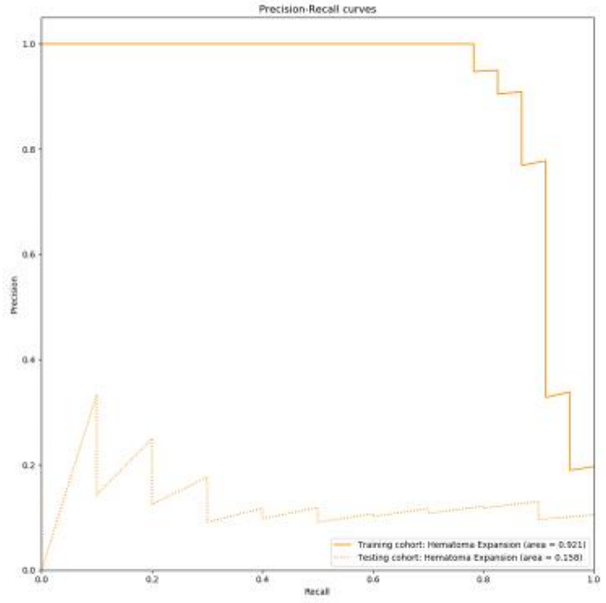

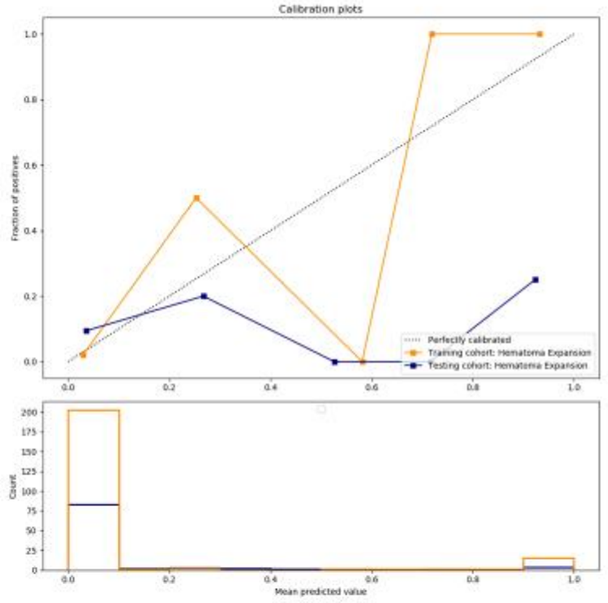

ROC curve

Precision-recall plot

Calibration plot

Supplementary Figure 4 Evaluation of predictive performance of hematoma expansion in prediction of hospital death on patients in the training and testing cohorts. Evaluation of predictive performances for hematoma expansion by ROC analysis, precision-recall plots, and calibration analysis.

Abbreviations: ROC, Receiver operating characteristic.

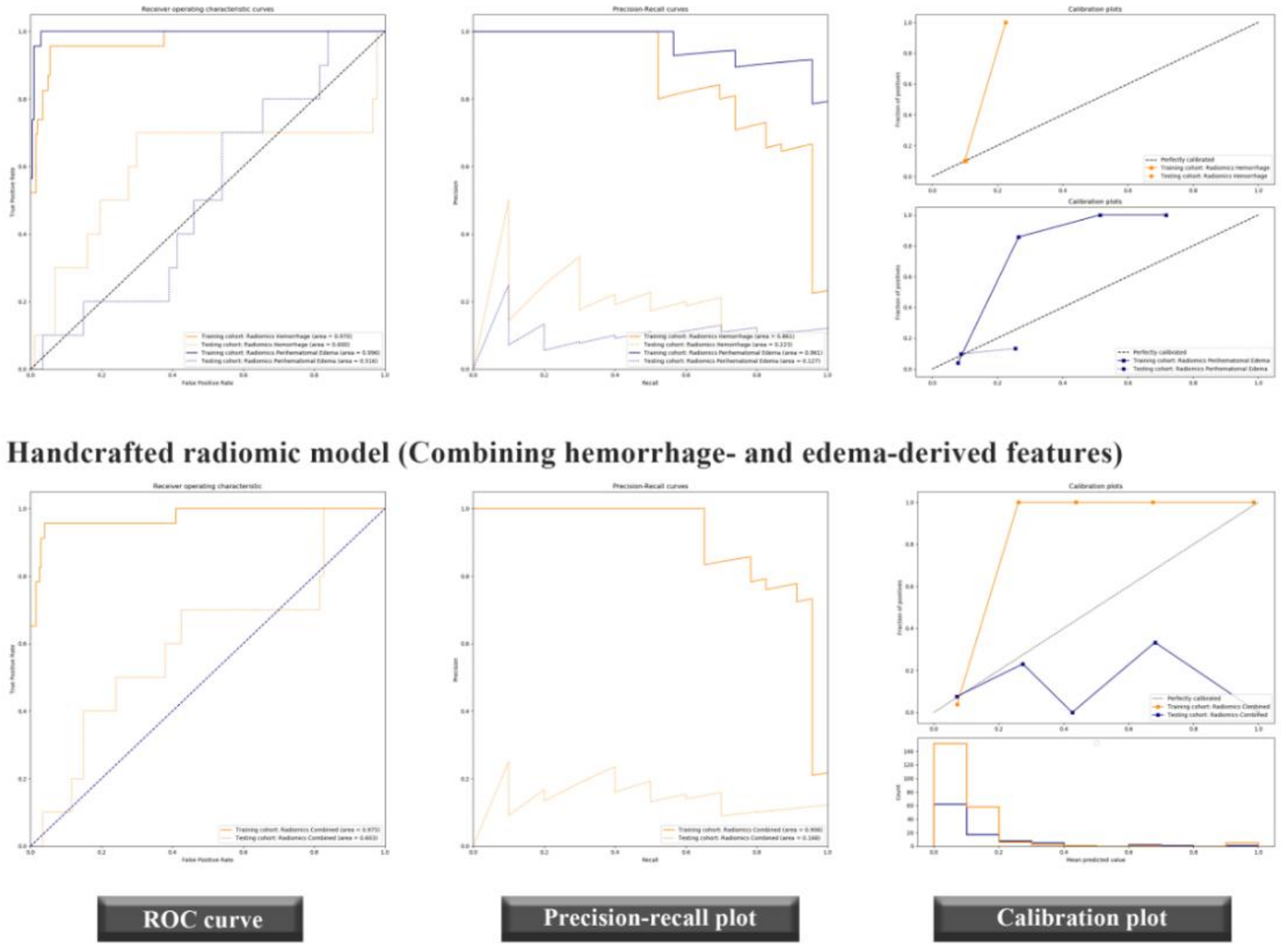

Supplementary Figure 5 Evaluation of predictive performance of handcrafted radiomics models in prediction of hospital death on patients in the training and testing cohorts. Evaluation of predictive performances for handcrafted radiomics models using hemorrhage-derived, perihematomal edema-derived, and combined features by ROC analysis, precision-recall plots, and calibration analysis. ROC, Receiver operating characteristic.

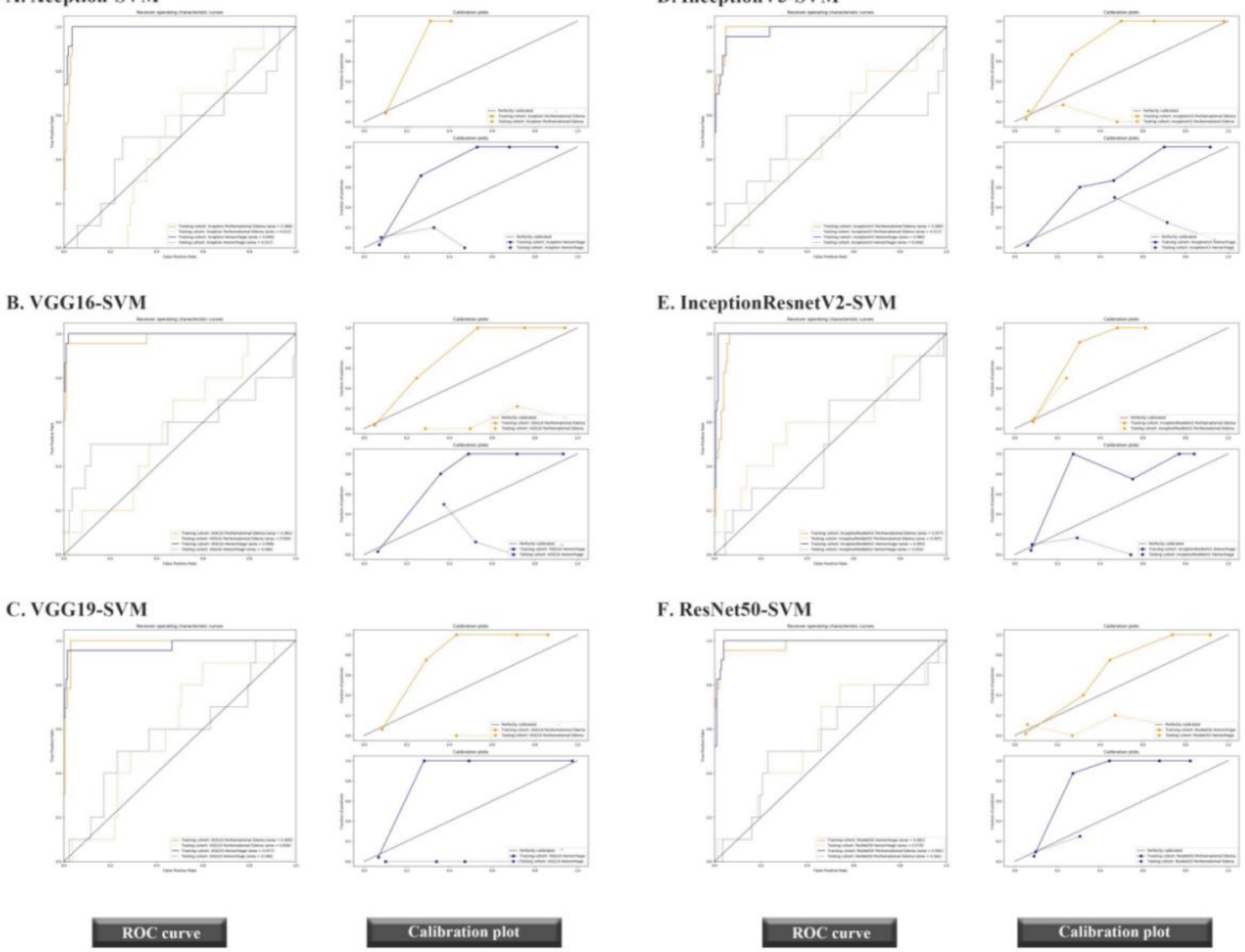

Supplementary Figure.S6. Evaluation of predictive performance of DL-SVM models on hemorrhage- or perihematomal edema-derived features in prediction of hospital death on patients in the training and testing cohorts. Evaluation of predictive performances for DL-SVM models using hemorrhage-derived or perihematomal edema-derived DL-associated features by ROC analysis and calibration analysis. DL, Deep learning; SVM, Support vector machine; ROC, Receiver operating characteristic.

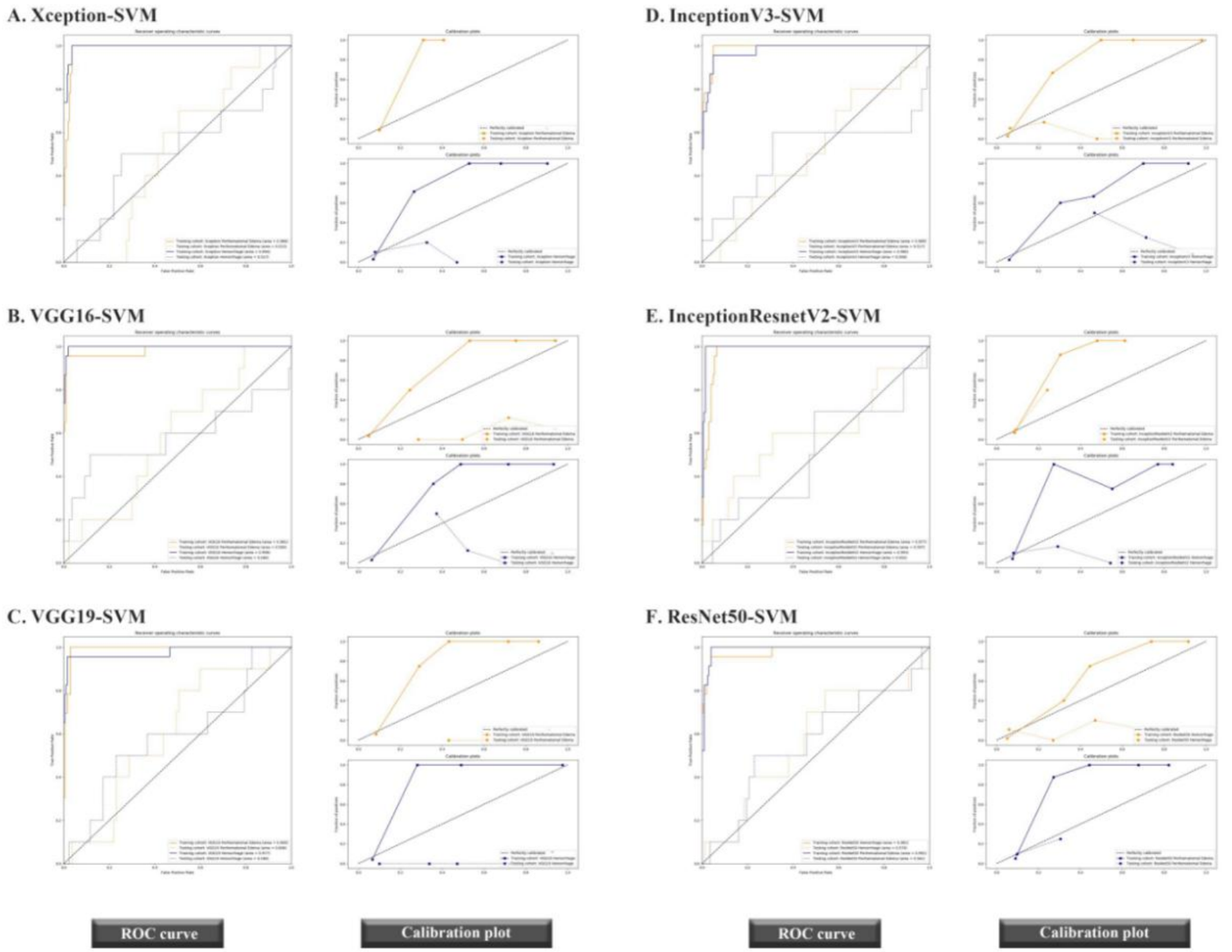

Supplementary Figure.S7. Evaluation of predictive performance of DL-SVM models combining hemorrhage- and perihematomal edema-derived features in prediction of hospital death on patients in the training and testing cohorts. Evaluation of predictive performances for DL-SVM models integrating hemorrhage- and perihematomal edema-derived features DL-associated features by ROC analysis and calibration analysis. DL, Deep learning; SVM, Support vector machine; ROC, Receiver operating characteristic.

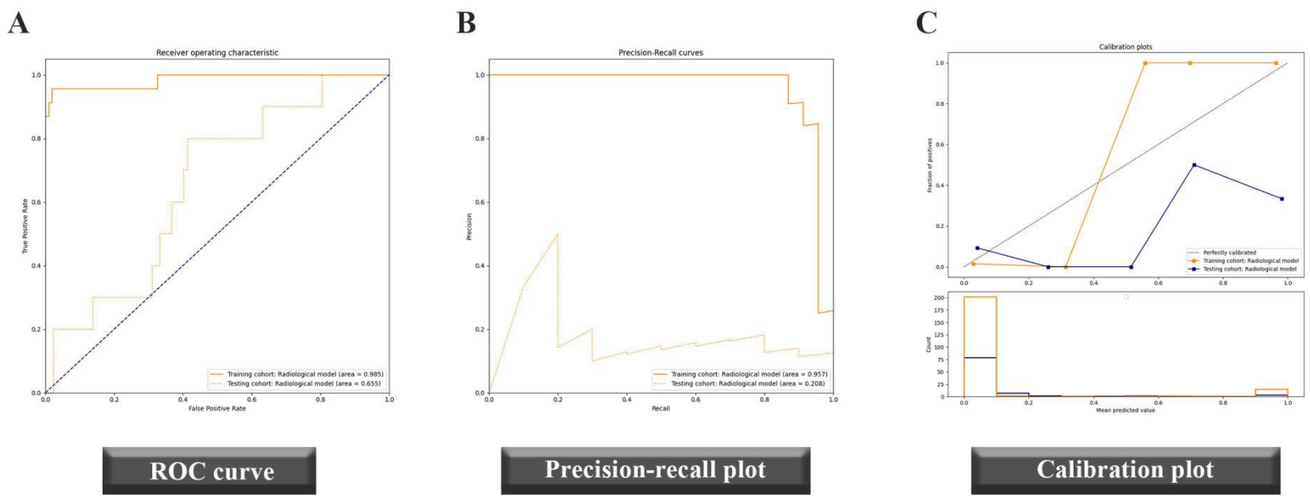

Supplementary Figure 8 Evaluation of predictive performance of the radiological model combining handcrafted radiomics and deep learning signatures on non-contrast enhanced CT imagesin prediction of hospital death on patients in the training and testing cohorts. Evaluation of predictive performances for the radiological model combining handcrafted radiomics and deep learning signatures by ROC analysis, precision-recall plot, and calibration analysis.DL, Deep learning; SVM, Support vector machine; ROC, Receiver operating characteristic.

Supplementary Table 1 Predictive performance of radiological models, clinical model and clinical-radiological model in prediction of early enlargement of spontaneous intracerebral hemorrhage on patients in the training cohort

Model	ROI	AUC	Accuracy	Sensitivity	Specificity	PPV	NPV	F1 score	AP score
Xception	Hemorrhage	0.911	82.67	84.34	81.69	72.92	89.92	0.782	0.873
	Perihematomal Edema	0.901	81.78	74.70	85.92	75.61	85.31	0.752	0.862
	Combined	0.889	83.11	74.70	88.03	78.48	85.62	0.765	0.865
VGG16	Hemorrhage	0.865	81.78	60.24	94.37	86.21	80.24	0.709	0.820
	Perihematomal Edema	0.901	82.22	75.90	85.92	75.90	85.92	0.759	0.875
	Combined	0.866	78.22	86.75	73.24	65.45	90.43	0.746	0.822
VGG19	Hemorrhage	0.876	78.22	84.34	74.65	66.04	89.08	0.741	0.852
	Perihematomal Edema	0.903	79.56	90.36	73.24	66.37	92.86	0.765	0.857
	Combined	0.827	74.22	78.31	71.83	61.90	85.00	0.691	0.775
ResNet50	Hemorrhage	0.889	79.56	90.36	73.24	66.37	92.86	0.765	0.851
	Perihematomal Edema	0.934	81.78	97.59	72.54	67.50	98.10	0.798	0.893
	Combined	0.841	74.67	89.16	66.20	60.66	91.26	0.722	0.792
InceptionV3	Hemorrhage	0.928	83.56	93.98	77.46	70.91	95.65	0.808	0.884
	Perihematomal Edema	0.968	90.67	87.95	92.25	86.90	92.91	0.874	0.950
	Combined	0.946	87.11	84.34	88.73	81.40	90.65	0.828	0.914
InceptionResNetV2	Hemorrhage	0.911	87.56	79.52	92.25	85.71	88.51	0.825	0.866
	Perihematomal Edema	0.925	80.89	95.18	72.54	66.95	96.26	0.786	0.887
	Combined	0.894	77.78	87.95	71.83	64.60	91.07	0.745	0.863
Handcrafted radiomics	Hemorrhage	0.902	82.67	74.70	87.32	77.50	85.52	0.761	0.855

	Perihematomal Edema	0.873	80.89	73.49	85.21	74.39	84.62	0.739	0.815
	Combined	0.895	80.00	86.75	76.06	67.92	90.76	0.762	0.834
Radiological model	/	0.933	87.56	83.13	90.14	83.13	90.14	0.831	0.877
Clinical model	/	0.829	79.11	74.70	81.69	70.45	84.67	0.725	0.792
Integrated model	/	0.973	92.00	93.98	90.85	85.71	96.27	0.897	0.943

ROI: Region of interest; AUC: Area under the receiver operating characteristic curve; PPV: Positive predictive value; NPV: Negative predictive value; AP: Average precision.

Supplementary Table 2 Handcrafted radiomics features of the whole volume selected for early enlargement of spontaneous intracerebral hemorrhage

ROI	Index	Filter [a]	Feature class	Feature
Hemorrhage	1	Wavelet (LHL)	GLSZM	Gray Level Non Uniformity Normalized
	2	Original [b]	First order [d]	Interquartile Range
	3	Wavelet (LLL) [c]	GLCM	Correlation
	4	Wavelet (LHH)	GLCM	Imc2
	5	Wavelet (LHL)	First order	Median
	6	Wavelet (LHL)	GLSZM	Zone Entropy
	7	Original	GLDM	Dependence Variance
	8	Wavelet (HHL)	GLDM	Dependence Non Uniformity Normalized
Perihematomal edema	1	Wavelet (HLL)	GLDM	Dependence Non Uniformity Normalized
	2	Wavelet (HLL)	GLCM	Idn
	3	Wavelet (HLL)	GLDM	Dependence Variance
	4	Wavelet (LLH)	GLRLM	Low Gray Level Run Emphasis
	5	Wavelet (LHH)	GLCM	Correlation
	6	Wavelet (LLH)	First order	Skewness
	7	Wavelet (HLL)	First order	Mean Absolute Deviation
	8	Wavelet (HHH)	GLSZM	Small Area Low Gray Level Emphasis

ROI, Region of interest; GLSZM, Gray Level Size Zone Matrix Features; GLCM, Gray Level Co-occurrence Matrix Features; GLDM, .Gray Level Dependence Matrix Features.

a: HLH, HLL, HHL, HHH and LLL, representative of high pass or low pass filter on the X, Y, Z three dimensions (H, high pass filter; L, low pass filter);

b: Original, original images without any filter used;

c: Wavelet, wavelet filtrated image;

d: First order, first order statistics.

Supplementary Table 3 Number of features selected and used in construction of deep learning-SVM models for prediction of early enlargement of spontaneous intracerebral hemorrhage

Feature extractor	ROI	Number of selected features
Xception	Hemorrhage	8
	Perihematomal edema	7
	Combined	6
VGG16	Hemorrhage	9
	Perihematomal edema	7
	Combined	9
VGG19	Hemorrhage	6
	Perihematomal edema	7
	Combined	8
ResNet50	Hemorrhage	3
	Perihematomal edema	8
	Combined	7
InceptionV3	Hemorrhage	7
	Perihematomal edema	10
	Combined	10
InceptionResNetV2	Hemorrhage	7
	Perihematomal edema	7
	Combined	7

SVM, Support vector machine; ROI, Region of interest.

Supplementary Table 4 Predictive performances of the radiological models constructed by features extracted from different layers of ResNet50 algorithm for prediction of early enlargement of spontaneous intracerebral hemorrhage

Layer	ROI	Training cohort								Testing cohort							
		AUC	Accuracy	Sensitivity	Specificity	PPV	NPV	F1 score	AP	AUC	Accuracy	Sensitivity	Specificity	PPV	NPV	F1 score	AP
Res2b	Hemorrhage	0.829	72.00	89.16	61.97	57.81	90.72	0.701	0.774	0.614	51.55	71.43	40.32	40.32	71.43	0.515	0.508
	Perihematomal edema	0.813	71.11	86.75	61.97	57.14	88.89	0.689	0.728	0.615	53.61	77.14	40.32	42.19	75.76	0.545	0.531
	Combined	0.795	79.11	51.81	95.07	86.00	77.14	0.647	0.761	0.667	65.98	54.29	72.58	52.78	73.77	0.535	0.608
Res3d	Hemorrhage	0.929	84.00	93.98	78.17	71.56	95.69	0.813	0.837	0.671	58.76	68.57	53.23	45.28	75.00	0.545	0.589
	Perihematomal edema	0.867	75.56	92.77	65.49	61.11	93.94	0.737	0.810	0.695	52.58	88.57	32.26	42.47	83.33	0.574	0.610
	Combined	0.848	76.44	90.36	68.31	62.50	92.38	0.739	0.776	0.753	60.82	77.14	51.61	47.37	80.00	0.587	0.749
Res4f	Hemorrhage	0.917	83.56	89.16	80.28	72.55	92.68	0.800	0.891	0.683	61.86	74.29	54.84	48.15	79.07	0.584	0.583
	Perihematomal edema	0.883	78.22	93.98	69.01	63.93	95.15	0.761	0.829	0.676	53.61	77.14	40.32	42.19	75.76	0.545	0.604
	Combined	0.925	80.44	96.39	71.13	66.12	97.12	0.784	0.888	0.748	59.79	91.43	41.94	47.06	89.66	0.621	0.641
Res5c	**Hemorrhage**	**0.889**	**79.56**	**90.36**	**73.24**	**66.37**	**92.86**	**0.765**	**0.851**	**0.747**	**63.92**	**82.86**	**53.23**	**50.00**	**84.62**	**0.624**	**0.686**
	Perihematomal edema	**0.934**	**81.78**	**97.59**	**72.54**	**67.50**	**98.10**	**0.798**	**0.893**	**0.659**	**46.39**	**71.43**	**32.26**	**37.31**	**66.67**	**0.490**	**0.575**
	Combined	**0.841**	**74.67**	**89.16**	**66.20**	**60.66**	**91.26**	**0.722**	**0.792**	**0.774**	**60.82**	**88.57**	**45.16**	**47.69**	**87.50**	**0.620**	**0.703**
FC1000	Hemorrhage	0.755	74.23	71.43	75.81	62.50	82.46	0.667	0.525	0.573	63.11	50.60	70.42	50.00	70.92	0.503	0.416
	Perihematomal edema	0.706	65.78	79.52	57.75	52.38	82.83	0.632	0.609	0.482	51.55	77.14	37.10	40.91	74.19	0.535	0.328
	Combined	0.755	69.78	77.11	65.49	56.64	83.04	0.653	0.624	0.576	54.64	48.57	58.06	39.53	66.67	0.436	0.447

RROI: Region of interest; AUC: Area under the receiver operating characteristic curve; PPV: Positive predictive value; NPV: Negative predictive value; AP: Average precision.

Supplementary Table 5 Clinical characteristics of patients with and without hospital death in the training and testing cohorts.

Characteristic	Training cohort (N = 225)			Testing cohort (N = 97)		
	Dead (n=23)	Alive (n=202)	P value	Dead (n=10)	Alive (n=87)	P value
Demographic characteristics						
Age, median (IQR), years	56 (20)	62 (26)	0.205	60 (45)	61 (25)	0.799
Gender, Male, No. (%)	15 (65.2)	115 (56.9)	0.446	7 (70.0)	54 (62.1)	0.740
Clinical features						
Time to arrival, median (IQR), h	1.6 (0.8)	1.5 (0.4)	0.600	1.6 (0.7)	1.6 (0.4)	0.361
Time to baseline CT, median (IQR), h	2.1 (0.3)	2.3 (0.7)	0.118	2.0 (0.5)	2.2 (0.7)	0.246
Systolic BP, median (IQR), mmHg	135 (46)	147 (44)	0.458	128 (49)	145 (44)	0.502
Diastolic BP, median (IQR), mmHg	90 (25)	86 (26)	0.239	72 (9)	85 (25)	0.889
Heart rate, median (IQR), bpm	82 (19)	80 (17)	0.675	85 (25)	80 (23)	0.705
GCS score, median (IQR)	11 (8)	13 (5)	0.440	13 (2)	14 (3)	0.920
NIHSS score, median (IQR)	10 (18)	6 (11)	0.750	12 (10)	5 (11)	0.445
Medical history						
Hypertension, No. (%)	10 (43.5)	100 (49.5)	0.584	5 (50.0)	39 (44.8)	1.000
Diabetes mellitus, Male, No. (%)	3 (13.0)	19 (9.4)	0.478	0 (0.0)	9 (10.3)	0.591
Dyslipidemia, No. (%)	0 (0.0)	6 (3.0)	1.000	0 (0.0)	2 (2.3)	1.000
Atrial fibrillation, No. (%)	0 (0.0)	5 (2.5)	1.000	0 (0.0)	1 (1.1)	1.000
Acute coronary syndrome, No. (%)	1 (4.3)	6 (3.0)	0.535	0 (0.0)	4 (4.6)	1.000
Ischemic stroke, No. (%)	0 (0.0)	2 (1.0)	1.000	0 (0.0)	2 (2.3)	1.000
Current smoking, No. (%)	3 (13.0)	10 (5.0)	0.135	1 (10.0)	3 (3.4)	0.358
Drinking history, No. (%)	1 (4.3)	5 (2.5)	0.480	0 (0.0)	0 (0.0)	1.000
Medication history						
Anti-platelet therapy, No. (%)	1 (4.3)	10 (5.0)	1.000	0 (0.0)	3 (3.4)	1.000
Anti-coagulant therapy, No. (%)	0 (0.0)	11 (5.4)	0.609	1 (10.0)	3 (3.4)	0.358

IQR, Interquartile range; BP, Blood pressure; NCCT, Non-contrast computed tomography; GCS, Glasgow score; NIHSS, National Institute of Health stroke scale.

Supplementary Table 6 Predictive performance of radiological models, clinical model and clinical-radiological model in prediction of hospital death on patients in the training cohort

Model	ROI	AUC	Accuracy	Sensitivity	Specificity	PPV	NPV	F1 score	AP score
Xception	Hemorrhage	0.994	96.44	95.65	96.53	75.86	99.49	0.846	0.955
	Perihematomal Edema	0.986	96.44	95.65	96.53	75.86	99.49	0.846	0.862
	Combined	0.957	93.33	86.96	94.06	62.50	98.45	0.727	0.805
VGG16	Hemorrhage	0.998	97.78	95.65	98.02	84.62	99.50	0.898	0.980
	Perihematomal Edema	0.981	98.22	91.30	99.01	91.30	99.01	0.913	0.935
	Combined	0.986	98.22	91.30	99.01	91.30	99.01	0.913	0.945
VGG19	Hemorrhage	0.977	97.78	91.30	98.51	87.50	99.05	0.894	0.937
	Perihematomal Edema	0.990	96.89	95.65	97.03	78.57	99.49	0.863	0.907
	Combined	0.993	96.00	95.65	96.04	73.33	99.49	0.830	0.937
ResNet50	Hemorrhage	0.981	95.56	91.30	96.04	72.41	98.98	0.808	0.924
	Perihematomal Edema	0.991	96.00	95.65	96.04	73.33	99.49	0.830	0.925
	Combined	0.982	94.67	91.30	95.05	67.74	98.97	0.778	0.921
InceptionV3	Hemorrhage	0.980	94.67	91.30	95.05	67.74	98.97	0.778	0.891
	Perihematomal Edema	0.989	95.11	95.65	95.05	68.75	99.48	0.800	0.922
	Combined	0.977	95.56	91.30	96.04	72.41	98.98	0.808	0.874
InceptionResNetV2	Hemorrhage	0.993	98.22	95.65	98.51	88.00	99.50	0.917	0.926
	Perihematomal Edema	0.977	93.78	95.65	93.56	62.86	99.47	0.759	0.794
	Combined	0.983	96.44	95.65	96.53	75.86	99.49	0.846	0.832
Handcrafted radiomics	Hemorrhage	0.970	94.22	91.30	94.55	65.63	98.96	0.764	0.861
	Perihematomal Edema	0.996	96.89	95.65	97.03	78.57	99.49	0.863	0.961

	Combined	0.975	95.56	91.30	96.04	72.41	98.98	0.808	0.906
Hematoma Expansion	/	0.969	96.00	86.96	97.03	76.92	98.49	0.816	0.921
Radiological model	/	0.985	97.33	91.30	98.02	84.00	99.00	0.875	0.957
Integrated model	/	0.992	96.00	95.65	96.04	73.33	99.49	0.830	0.932

ROI, Region of interest; AUC, Area under the receiver operating characteristic curve; PPV, Positive predictive value; NPV, Negative predictive value; AP, Average precision.

Supplementary Table 7 Handcrafted radiomics features of the whole volume selected for hospital death

ROI	Index	Filter [a]	Feature class	Feature
Hemorrhage	1	Wavelet (LLH) [c]	GLCM	Idmn
	2	Wavelet (LHH)	GLCM	Imc1
	3	Wavelet (HHL)	GLDM	Dependence Entropy
	4	Wavelet (HLL)	First order [d]	Maximum
	5	Original [b]	GLDM	Dependence Non Uniformity Normalized
	6	Wavelet (LHH)	GLRLM	High Gray Level Run Emphasis
Perihematomal edema	1	Original	GLCM	Sum Entropy
	2	Original	Shape	Elongation
	3	Wavelet (HHL)	GLDM	Dependence Entropy
	4	Wavelet (LHH)	First order	Entropy
	5	Wavelet (LHH)	First order	Variance
	6	Original	GLCM	Correlation

ROI, Region of interest; GLSZM, Gray Level Size Zone Matrix Features; GLCM, Gray Level Co-occurrence Matrix Features; GLDM, .Gray Level Dependence Matrix Features.

a: HLH, HLL, HHL, HHH and LLL, representative of high pass or low pass filter on the X, Y, Z three dimensions (H, high pass filter; L, low pass filter);

b: Original, original images without any filter used;

c: Wavelet, wavelet filtrated image;

d: First order, first order statistics.

Supplementary Table 8 Number of features selected and used in construction of deep learning-SVM models for prediction of hospital death

Feature extractor	ROI	Number of selected features
Xception	Hemorrhage	5
	Perihematomal edema	6
	Combined	7
VGG16	Hemorrhage	8
	Perihematomal edema	6
	Combined	8
VGG19	Hemorrhage	7
	Perihematomal edema	6
	Combined	7
ResNet50	Hemorrhage	7
	Perihematomal edema	6
	Combined	7
InceptionV3	Hemorrhage	6
	Perihematomal edema	7
	Combined	5
InceptionResNetV2	Hemorrhage	7
	Perihematomal edema	5
	Combined	9

SVM, Support vector machine; ROI, Region of interest.

Supplementary Table 9 Predictive performances of the radiological models constructed by features extracted from different layers of ResNet50 algorithm for prediction of hospital death

Layer	ROI	Training cohort								Testing cohort							
		AUC	Accuracy	Sensitivity	Specificity	PPV	NPV	F1 score	AP	AUC	Accuracy	Sensitivity	Specificity	PPV	NPV	F1 score	AP
Res2b	Hemorrhage	0.983	95.56	95.65	95.54	70.97	99.48	0.815	0.847	0.608	71.13	50.00	73.56	17.86	92.75	0.263	0.196
	Perihematomal edema	0.985	96.00	95.65	96.04	73.33	99.49	0.830	0.859	0.620	76.29	40.00	80.46	19.05	92.11	0.258	0.172
	Combined	0.980	96.89	91.30	97.52	80.77	98.99	0.857	0.862	0.646	73.20	50.00	75.86	19.23	92.96	0.278	0.228
Res3d	Hemorrhage	0.996	98.67	95.65	99.01	91.67	99.50	0.936	0.965	0.548	70.10	50.00	72.41	17.24	92.65	0.256	0.193
	Perihematomal edema	0.983	96.00	91.30	96.53	75.00	98.98	0.824	0.851	0.549	67.01	50.00	68.97	15.63	92.31	0.238	0.193
	Combined	0.986	97.33	95.65	97.52	81.48	99.49	0.880	0.853	0.602	79.38	30.00	85.06	18.75	91.36	0.231	0.144
Res4f	Hemorrhage	0.986	96.89	95.65	97.03	78.57	99.49	0.863	0.866	0.566	62.89	40.00	65.52	11.76	90.48	0.182	0.230
	Perihematomal edema	0.997	97.78	95.65	98.02	84.62	99.50	0.898	0.973	0.509	78.35	40.00	82.76	21.05	92.31	0.276	0.133
	Combined	0.992	95.56	95.65	95.54	70.97	99.48	0.815	0.945	0.628	68.04	60.00	68.97	18.18	93.75	0.279	0.221
Res5c	**Hemorrhage**	**0.981**	**95.56**	**91.30**	**96.04**	**72.41**	**98.98**	**0.808**	**0.924**	**0.570**	**67.01**	**40.00**	**70.11**	**13.33**	**91.04**	**0.200**	**0.173**
	Perihematomal edema	**0.991**	**96.00**	**95.65**	**96.04**	**73.33**	**99.49**	**0.830**	**0.925**	**0.561**	**71.13**	**50.00**	**73.56**	**17.86**	**92.75**	**0.263**	**0.149**
	Combined	**0.982**	**94.67**	**91.30**	**95.05**	**67.74**	**98.97**	**0.778**	**0.921**	**0.705**	**64.95**	**60.00**	**65.52**	**16.67**	**93.44**	**0.261**	**0.254**
FC1000	Hemorrhage	0.898	71.11	91.30	68.81	25.00	98.58	0.393	0.613	0.557	63.92	30.00	67.82	9.68	89.39	0.146	0.120
	Perihematomal edema	0.768	66.22	73.91	65.35	19.54	95.65	0.309	0.436	0.455	52.58	20.00	56.32	5.00	85.96	0.080	0.098
	Combined	0.907	78.22	82.61	77.72	29.69	97.52	0.437	0.602	0.626	67.01	40.00	70.11	13.33	91.04	0.200	0.139

ROI, Region of interest; AUC, Area under the receiver operating characteristic curve; PPV, Positive predictive value; NPV, Negative predictive value; AP, Average precision.